Quarterly Progress Report 1

Radar Studies of the Moon

15 February 1967

Issued 28 February 1967

Prepared for the U.S. National Aeronautics and Space Administration
under Contract NSR 22-009-106 by

Lincoln Laboratory

MASSACHUSETTS INSTITUTE OF TECHNOLOGY

Lexington, Massachusetts

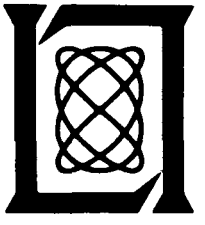

FOREWORD

This is the fifth quarterly progress report under Contract NSR-22-009-106 between the National Aeronautics and Space Administration and Lincoln Laboratory. Previous quarterly progress reports will be referred to as QPR (1966:1) through QPR (1966:4) in this report.

Significant progress has been made during this quarter in an unambigucus mapping method suitable for wide-beam antennas as briefly described in QPR (1966:3). A coarse resolution contour map of the whole lunar disk has been obtained at 23 cm and is described in Sec. I. Section II describes progress in delay-Doppler mapping at 3.8 cm. The difficulties with the data analysis have now been overcome and a number of radar reflectivity maps have been produced, some of which are shown and discussed in this report. Section III describes progress in the development of the 8-mm radar system.

CONTENTS

RADAR STUDIES OF THE MOON

I. UNAMBIGUOUS COHERENT RADAR MAPPING AT 23 CM

A. Introduction

The delay-Doppler technique employed to map the moon at 3.8-cm wavelength, using the Haystack antenna, has certain limitations because the resolution deteriorates somewhat near the subradar point. Since the subradar point migrates over the lunar surface in the course of time, this difficulty can be largely overcome by making observations on many different days. However, since the subradar point moves only some ±6° in selenographic longitude and latitude, there may still remain a certain area near the center of the moon which can be mapped only coarsely. This circumstance provides one reason for exploring possible alternatives to the delay-Doppler technique.

Delay-Doppler mapping is inherently twofold ambiguous since for a given appropriately constrained coordinate pair there will nearly everywhere be two corresponding points on the surface. This difficulty is easily avoided at Haystack at 3.8 cm by using the narrow polar diagram of the antenna to resolve the ambiguity. At Millstone, however, where at 23-cm wavelength the half-power beamwidth of the antenna is larger than the angular radius of the moon, unambiguous mapping cannot be carried out by the simple delay-Doppler technique. This provides a second incentive to developing alternative mapping methods.

The flexibility in the choice of polarizations both for transmission and for reception available at Millstone at 23 cm (Hagfors, 1967) makes it desirable to devise an unambiguous mapping technique so that the depolarizing properties of distinctive features can be obtained. In view of the lack of a similar polarization flexibility at the Haystack facility, it becomes particularly important to carry out moderate or high resolution polarization experiments with the 23-cm Millstone radar.

Additional arguments for exploring mapping techniques other than those based on delay and Doppler, although not of direct interest in the present moon program, derive from the desirability of mapping planetary surfaces. The angular diameters of the planets are so small that one cannot, in the foreseeable future, hope to resolve them with an antenna polar diagram. This means that the ambiguities of the delay-Doppler technique cannot easily be resolved in planetary observations. Hence, if unambiguous mapping methods can be devised for lunar observations without making use of delay-Doppler and beam resolution, it appears that these might well find some applications in planetary mapping as well.

The two-dimensional mapping procedure described in Sec. I-B can be shown to be related to a technique for obtaining delay-spread information from spectral analysis (Carpenter, 1964) which has been used rather extensively to derive information about planetary surfaces (Evans, et al., 1966).

In QPR (1966:3) the computational formulas of the mapping method were developed in some detail. Nevertheless, in Sec. I-B we shall review some of the basic principles of the method and particularly discuss various choices of parameters to be used. In Sec. I-C we then proceed

to describe a computer program which has been developed to produce two-dimensional maps. Section I-D discusses some observations which have been made and shows an example of a map produced from these observations.

B. Discussion of Mapping Technique

In this section we give the principles of the mapping method and derive the necessary formulas from first principles. In particular we investigate the effect on the final map of finite-width strips in the strip distribution and of making observations only at a discrete set of strip directions. We then proceed to discuss some special problems relating to the application of the mapping method to lunar returns. Finally in this section a relationship is established between the two-dimensional mapping procedure described here and a method that has found some application in radar astronomy whereby the power-delay relationship of lunar and planetary returns may be determined from a single frequency spectrum.

1. Basic Principles of Method

Let the power reflected or emitted per unit surface area (projected) be denoted by $f(\xi; \eta)$. The power arising from a strip which makes an angle φ with the η-axis, which is at a distance x from the origin and which has a width Δx is given by (Fig. 1)

$$W(r, \varphi) = \int_{r-(\Delta x/2)}^{r+(\Delta x/2)} dx' \int_{-\infty}^{+\infty} dy'\, f(x' \cos\varphi - y' \sin\varphi;\ y' \cos\varphi + x' \sin\varphi) \quad . \tag{1}$$

For the sake of these introductory arguments we shall assume that by measurement we can derive the quantity

$$U(r, \varphi) = \lim_{\Delta x \to 0} \left(\frac{W(r, \varphi)}{\Delta x} \right) = \int_{-\infty}^{+\infty} dy'\, f(r \cos\varphi - y' \sin\varphi;\ y' \cos\varphi + r \sin\varphi) \quad . \tag{2}$$

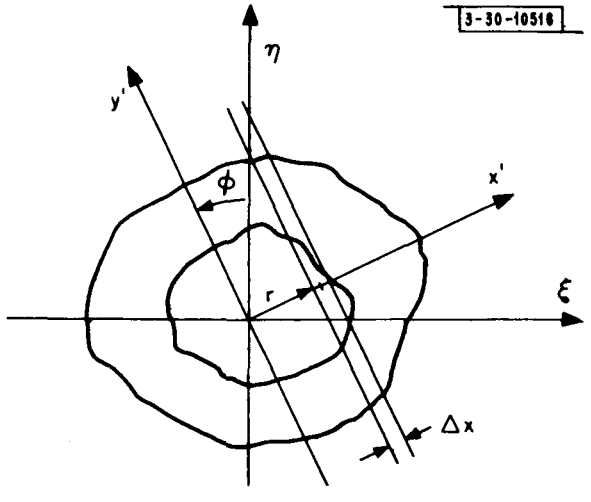

Fig. 1. Strip superimposed on ξ-η plane.

The two-dimensional power distribution over the surface, $f(\xi;\eta)$, may be derived from $U(r,\varphi)$ as follows: Assume that $f(\xi;\eta)$ may be represented as a double Fourier integral

$$f(\xi;\eta) = \iint R(u;v)\, e^{-2\pi i(u\xi+v\eta)}\, du\, dv \quad . \tag{3}$$

By substituting Eq. (3) into Eq. (2) and performing the integration over y' gives

$$U(r,\varphi) = \iint du\, dv\, R(u;v)\, e^{-2\pi i(u\cos\varphi+v\sin\varphi)r}\, \delta(v\cos\varphi - w\sin\varphi) \tag{4}$$

where δ is Dirac's delta function. Integration over v and substitution of $t = w/\cos\varphi$ gives

$$U(r,\varphi) = \int dt\, R(t\cos\varphi;\ t\sin\varphi)\, e^{-2\pi irt} \quad . \tag{5}$$

Simple Fourier inversion of this gives

$$R(t\cos\varphi;\ t\sin\varphi) = \int dr\, U(r,\varphi)\, e^{2\pi irt} \quad . \tag{6}$$

Since Eq. (6) determines $R(u;v)$ in the whole of the (u,v) plane, the power distribution $f(\xi;\eta)$ can be found by simple substitution into Eq. (3). In so doing, it is convenient to change the variables of integration to polar coordinates first:

$$\begin{aligned} f(\xi;\eta) &= \iint R(t\cos\varphi;\ t\sin\varphi)\, t\, e^{-2\pi it(\xi\cos\varphi+\eta\sin\varphi)}\, dt\, d\varphi \\ &= \int_0^{2\pi} d\varphi \int_0^{\infty} t\, dt\, e^{-2\pi it(\xi\cos\varphi+\eta\sin\varphi)} \int_{-\infty}^{+\infty} dr\, U(r,\varphi)\, e^{2\pi irt} \end{aligned} \tag{7}$$

This solves our original problem. The function $R(u;v)$ which we introduced is shown elsewhere to be related to the two-dimensional correlation function of the diffraction pattern of the source (Bracewell, 1962). As such it may be measured directly by spaced antennas or by a single antenna, provided in the latter case that the diffraction pattern moves over the antenna without change.

In the application of these ideas to lunar radar mapping, we have to measure strip distributions with finite resolution, and not necessarily with the rectangular filter indicated in Eq. (1). Let us assume that the power spectral response of the filter actually used is denoted by $g(r)$. This means that Eq. (1) is replaced by

$$W(r,\varphi) = \iint_{-\infty}^{+\infty} g(x'-r)\, f(x'\cos\phi - y'\sin\varphi;\ y'\cos\varphi + x'\sin\varphi)\, dx'\, dy' \tag{1a}$$

and it is not possible to pass to the limit of infinitely narrow filters in practice.

Suppose that we use Eq. (7) with $W(r,\varphi)$ rather than with $U(r,\varphi)$. The resulting power density, which we now denote by $P(\xi;\eta)$, must be some sort of smoothed average of $f(\xi;\eta)$. We now derive the relationship between the smoothing function and the filter function $g(x)$. Substitution of Eq. (1a) into Eq. (7) and transformation of the integration variable gives

$$P(\xi;\eta) = \int_0^{2\pi} d\varphi \int_0^{\infty} t\, dt\, e^{-2\pi i r(\xi\cos\varphi+\eta\sin\varphi)} \int_{-\infty}^{+\infty} dr\, e^{2\pi i r t}$$

$$\cdot \iint_{-\infty}^{+\infty} g(x'-r)\, f(x'\cos\varphi - y'\sin\varphi;\ y'\cos\varphi + x'\sin\varphi)\, dx'\, dy'$$

$$= \iint dx\, dy\, f(x,y)\, G(x-\xi,\ y-\eta) \qquad (8)$$

where $G(x, y)$ is a two-dimensional smoothing function defined by

$$G(x;y) = 2\pi \int_0^{\infty} r\, dr \int_{-\infty}^{+\infty} d\rho\ g(\rho)\ J_0\left(r\sqrt{x^2+y^2}\right) e^{-2\pi i r\rho} \qquad (9)$$

where J_0 is a zero-order Bessel function. As an example, consider the case corresponding to Eq. (1) or

$$g(\rho) = 1 \qquad |\rho| < \Delta x/2$$

$$= 0 \qquad \text{otherwise} \quad .$$

This gives

$$G(x,y) = 2\Big/\sqrt{\pi^2\Delta x^2 - x^2 - y^2} \qquad x^2+y^2 < \pi^2\Delta x^2$$

$$= 0 \qquad \text{otherwise} \quad . \qquad (10)$$

The smoothing function of Eq. (11) is unsatisfactory since it weights points removed from the origin more heavily than ones near the origin. As another example, consider the case

$$g(\rho) = e^{-\rho^2/2\Delta x^2}$$

which gives

$$G(x,y) = [1/(\Delta x\sqrt{2\pi})]\ e^{-(x^2+y^2)/8\pi^2\Delta x^2} \quad . \qquad (11)$$

This smoothing function appears to be satisfactory. The $g(\rho)$ actually used in the analysis of data below is of the intermediate form $(\sin\alpha\ \rho/\alpha\rho)^2$ but, unfortunately, we have not yet found an analytical expression for the corresponding $G(x, y)$.

Having explored the effect of filtering the strip distribution, we must next turn our attention to the effect of not knowing $W(r, \varphi)$ for all φ but only for a discrete set of values. This is all we can ever hope to achieve in an actual experimental situation. Even a strictly discrete set of values of φ cannot be obtained in the case of lunar radar observations since the direction φ is changing continuously during a run and an averaging over a certain sector of angles φ will automatically be made.

In the case of a discrete set of equidistantly spaced angles φ_i one can express the effect of the discrete angle sampling as a smoothing, as in Eq. (8). The smoothing function $G(x, y)$ now, however, is of the form

$$G(x, y) = \frac{1}{4\pi^2} \sum_{i=1}^{N} \frac{1}{(x \cos \varphi_i + y \sin \varphi_i)^2} \quad . \tag{12}$$

It follows that the sidelobe rejection is in direct proportion to the number of runs N combined to produce the map.

2. Application of Mapping Technique to Lunar Radar Studies

In lunar radar observations, the filtered strip distribution corresponding to $W(r, \varphi)$, of Eq. (1a) is obtained by coherently processing the echoes from the moon. The analysis program currently available computes the frequency spectrum of a concurrent sequence of complex samples, the duration T of this sequence being determined by the required filter width of the smoothing function g(x); that is, $\Delta f = 1/T$. Since all the samples are weighted equally, the corresponding g(x) is a $(\sin x/x)^2$ frequency response. A number of spectra obtained from such sequences are then added incoherently to reduce the noise. The angle φ in the lunar observations corresponds to the angle between the projection of the lunar meridian through the subradar point and the instantaneous apparent libration axis. The libration axis is defined as the locus of points across the disk of the moon which has the same Doppler frequency as the center of the moon. The subradar point in the course of time will move across the disk of the moon as a result of both optical librations and because of the diurnal motion of the observer. The instantaneous libration axis will always be normal to this curve. If the direction of motion of the subradar point changes by at least 180° in the course of a day's observation, then a complete map can be produced. The rotation of the libration axis by as much as 180° may therefore be expected to occur most frequently when the moon is at a high declination.

The motion of the subradar point across the surface of the moon causes the radar appearance of the moon to change somewhat in the course of an observation. If the reflectivity does not change too rapidly with the orientation of the observer with respect to the surface, this is not too serious. However, the polarized return has a very bright highlight near the subradar point and this highlight does not move with the surface, but rather remains fixed with respect to the observer. In order to avoid this difficulty, we have observed primarily in depolarized radiation so far. When it is required to observe in polarized radiation we have carefully removed the "glare" near the subradar point by range gating.

The center-to-limb Doppler-frequency offset is changing with time. In order to retain a fixed resolution with respect to the lunar surface, the coherent integration time T should be varied in inverse proportion to the center-to-limb Doppler shift for the run under consideration. This means that Δf is always a fixed fraction of the total limb-to-limb Doppler spread of the moon.

Let us finally under this section qualitatively discuss the limitations of the coherent mapping method as far as angular resolution on the moon is concerned, and what precautions must be taken to achieve this angular resolution. From experience gained through the use of the delay-Doppler technique at 3.8 cm at Haystack, it appears that a resolution of 1 to 2 km can be achieved near the subradar point. At 23 cm a comparable resolution can be obtained, but the maps will be somewhat noisier because the coherent integration interval must be seven times longer than at 3.8 cm. Since the angle φ (direction of the libration axis) is changing fairly rapidly, it means

that incoherent addition of several spectra to remove noise may not be possible. Because of the difficulties with the specular component, the mapping cannot be carried out in polarized radiation near the subradar point. In depolarized radiation, however, this region can be mapped, since the variation of reflectivity with angle of incidence is sufficiently slow. The analysis should be carried out with reference to a fixed point on the moon and not with respect to the subradar point as in the example analyzed below. This refinement is necessary only when one strives to achieve extreme resolution.

3. Simplification When Distribution is Circularly Symmetric

Before leaving this discussion of the basic principles of the method it is worthwhile to examine a particular case: that for which the power distribution (reflectivity) is circularly symmetric about the subradar point. Derivations of power-delay relationships for the moon and some of the planets have been made rather extensively in the past on the basis of measurements of frequency spectra (Carpenter, 1964). We now very briefly show that the mapping method described above reduces to the same derivation when the assumption of circular symmetry is made. In Eq. (8), $U(r, \varphi)$ or rather $W(r, \varphi)$ is independent of φ. This means that the integration over φ can be carried out and we obtain

$$P(\xi;\eta) = P(\rho) = 2\pi \int_0^\infty t\, dt\, J_0(t\rho) \int_{-\infty}^{+\infty} W(r)\, e^{2\pi i r t}\, dr$$

$$= 4\pi \int_0^\infty t\, dt\, J_0(t\rho) \int_0^{+\infty} W(r) \cos 2\pi r t\, dr \quad . \tag{13}$$

Here $\rho = \sqrt{\xi^2 + \eta^2}$ and $J_0(\ )$ is again the zero-order Bessel function. The conversion is usually quoted in terms of a single rather than a double integral. To show the equivalence we note that

$$\int_0^\infty t\, dt\, J_0(t\rho) \cos 2\pi r t = \frac{1}{2\pi} \frac{\partial}{\partial r} \int_0^\infty dt \sin 2\pi r t J_0(t\rho) \quad . \tag{14}$$

Substituting this back into Eq. (13) and integrating by parts, we obtain

$$F(\rho) = -\text{const} \int_0^\infty dr \int_0^\infty \frac{dW}{dr} \sin 2\pi r t J_0(t\rho)\, dt$$

$$= -\text{const} \int_\rho^\infty dr\, \frac{dW}{dr} \frac{1}{\sqrt{r^2 - \rho^2}} \quad . \tag{15}$$

This is essentially the form given by Carpenter in analyzing his Venus results (Carpenter, 1964). The procedure suggested by Eq. (13), however, may be preferable, since it does not involve the computation of derivatives in the observed spectral distribution. Since the integral over r in Eq. (14) is proportional to the signal autocorrelation function, further practical advantages may be gained if this function is measured directly.

TABLE I

LIST OF OBSERVATIONS

Date	No. Runs	Transmitter Polarization	Receiver Polarization	Comment
6/21/66	18	Circular	Circularly depolarized	Successful
10/3/66	18	Circular	Circularly depolarized	Unsuccessful
11/5/66	17	Circular	Circularly polarized + depolarized	Successful
12/27/66	27	Circular	Circularly polarized + depolarized	Successful

C. Description of Observational Results and Their Analysis

Observations of the moon at 23 cm using the Millstone radar for coherent mapping purposes were made on four different occasions. Some particulars of the observations are given in Table I. The three successful runs have been analyzed and it was found that the depolarized reflectivity maps were very similar, although the last set of runs appears to give maps which are less noisy than the previous runs. This is probably due primarily to the greater number of runs in the December observation, but it is also due to the better polarization rejection in the last observations. In what follows we shall therefore describe in detail the analysis of the December data and show the depolarized map which resulted from them.

1. Observations

The date 27-28 December 1966 was chosen for the experiment because of the favorable motion of the libration axis. The computation of the so-called Doppler angle C which corresponds to the angle φ in the analysis above was derived from the standard ephemeris program available on site. Figure 2 shows the variation of the Doppler angle with time. Also shown in the same diagram is the altitude of the moon as a function of time.

Sequences of 1-msec pulses were transmitted at interpulse periods 30, 36, or 48 msec depending on the speed of libration and on the range of the target. The local oscillators of the receivers were steered in accordance with ephemeris predictions to compensate for the Doppler offset of the center of the moon in the usual manner. A circularly polarized wave was transmitted and both circularly polarized waves were received in separate receivers. In both channels the in-phase and quadrature components (after translation to zero mean-Doppler) were sampled, each at a rate of 1 kHz in a "window" 18 msec wide. This "window" was locked to the motion of the echo on the time base. Of the 18 samples, 12 contain signal and the remaining 6 noise only. No calibration pulse was inserted on the time base, since the mapping program does not depend on absolute signal levels. The samples were digitized to 6-bit words and stored on magnetic tape. The duration of each run was five minutes. During this time interval, the libration axis

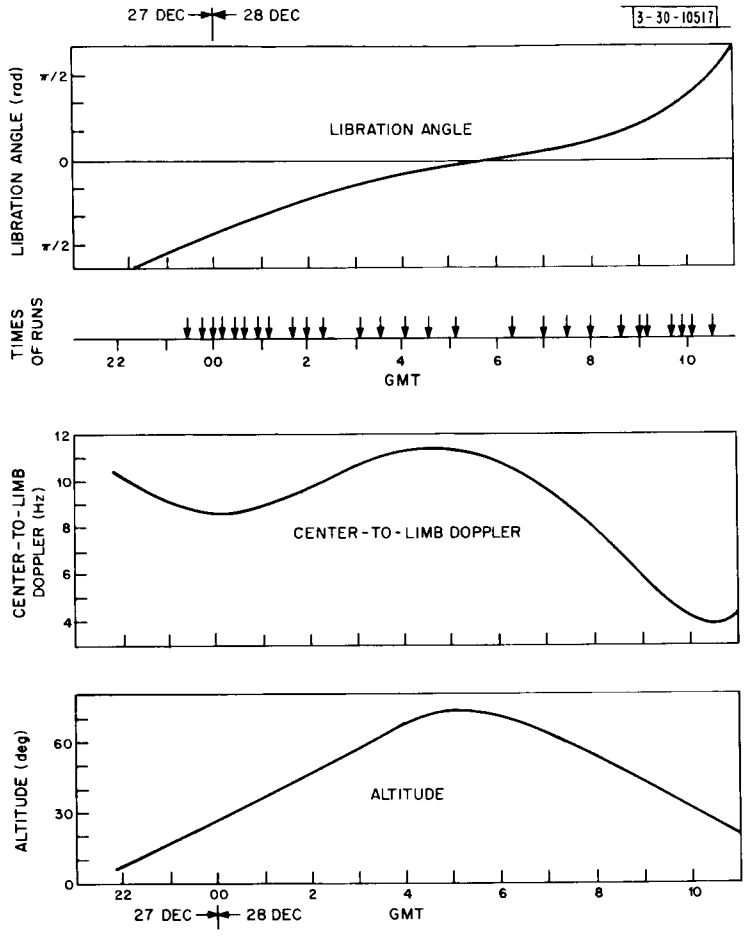

Fig. 2. Variation of altitude, Doppler angle and center-to-limb Doppler with time.

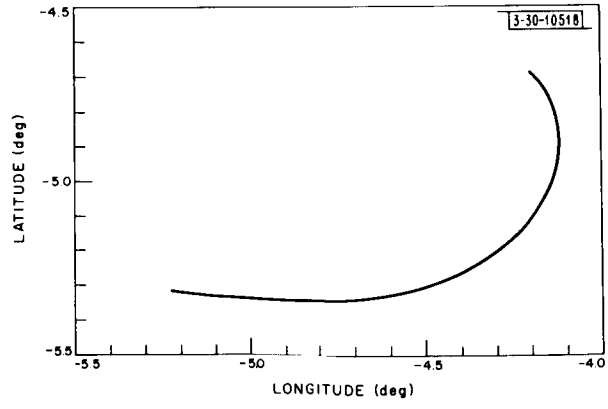

Fig. 3. Motion of subradar point during observations.

rotated by at most 4°. In the great majority of runs, the rotation was less than 2°. This was not considered serious, since only relatively coarse resolution was desired in the maps. For finer resolution, each five-minute run will have to be subdivided and each subdivision must be treated as a separate run.

The computation of frequency spectra and the antenna pointing were done in reference to the subradar point and not with reference to a definite point on the lunar surface. This will cause some blurring of the data. In order to determine the degree of blurring, the motion of the subradar point in selenographic latitude and longitude during the observational period was plotted in Fig. 3. As can be seen, the amount of motion does not exceed 1.5° in selenographic latitude or longitude or in other words it is less than about 45 km on the surface.

The 18 range samples of the 27 runs taken on 27-28 December were frequency analyzed into 61 equally spaced frequencies so that 51 of these correspond to the diameter of the moon. The width of the $(\sin x/x)^2$ was chosen so that the first zero on either side of the center of the filter coincided with the centers of the neighboring filters. Table II lists in detail the parameters of the 27 runs. The column listed as "Starting Frequency" refers to the frequency offset of the lowest frequency filter with respect to the subradar point. The other entries should be self-explanatory.

2. Combination of Frequency Spectra to Produce Map

The combination of the frequency spectra from various runs into a map follows very closely the development of Sec. III of QPR (1966:3). Only the depolarized circularly polarized map will be discussed as an illustration in the present report.

The program is basically divided into two parts, the first part computing and storing the smoothed correlation function R_f [see QPR (1966:3), Eq. (26)], the second part computing the reflectivity $P(\xi,\eta)$ as a function of the coordinates ξ and η. A third part of the program determines contours of constant reflectivity as a function of ξ and η from the reflectivity matrix.

Consider the first part of the analysis program. For each run characterized by a certain Doppler angle φ, a number (18) of frequency spectra containing 61 frequencies is read in from magnetic tape previously generated by the spectral analysis program. The mean power at each frequency due to noise alone is computed from the six ranges not containing an echo. This mean noise level is subtracted from the signal-containing range samples. For the depolarized component which we are concerned about in the present report, all the signal-containing frequency spectra corresponding to different ranges were added. For the polarized component, the "glare" from the subradar point can be avoided by omitting one or two of the first range boxes. In other cases we may want to be concerned with only a single range ring as will be explained below. The ranges of interest can be freely specified in the analysis program.

The averaged frequency spectra were used to compute the R_f, the complex autocorrelation of the signal for each run. The smoothing factor "Filt" occurring in QPR (1966:3), Eq. (26), was chosen to be equal to 0.25 as a result of some experimentation with the data. This corresponds essentially to trebling the filter widths of the frequency spectra to reduce noise. Hence, in the final output, there will be only the equivalent of 17 filter widths along the diameter of the moon. This first part of the program also requires for each run (see Table II) the input of the

TABLE II

PARAMETERS RELATING TO 27-28 DECEMBER MOON RUNS

Run No.	Time (GMT)	Doppler Angle (degrees)	Center-to-Limb Doppler (Hz)	Frequency Spacing (Hz)	Starting Frequency (Hz)	Interpulse Period (msec)	Interpulse/ Coherent Integration
1	2325	−90.695	8.783	0.3520	−10.55	36	79
2	2340	−85.306	8.683	0.3475	−10.42	36	80
3	2350	−79.871	8.636	0.3455	−10.35	36	80
4	0005	−76.256	8.633	0.3455	−10.35	48	60
5	0020	−70.897	8.669	0.3470	−10.40	48	60
6	0035	−65.671	8.751	0.3505	−10.49	48	59
7	0050	−60.631	8.874	0.3550	−10.64	48	59
8	0105	−55.812	9.031	0.3610	−10.83	48	58
9	0140	−45.548	9.494	0.3795	−11.38	30	88
10	0155	−41.581	9.717	0.3890	−11.65	30	86
11	0215	−36.674	10.020	0.408	−12.23	30	82
12	0305	−26.094	10.721	0.4290	−12.87	36	65
13	0330	−21.536	10.998	0.440	−13.19	36	63
14	0400	−16.550	11.232	0.449	−13.48	36	62
15	0430	−11.963	11.336	0.454	−13.62	36	61
16	0505	− 6.947	11.274	0.452	−13.53	36	62
17	0620	+ 3.445	10.423	0.417	−12.50	36	67
18	0655	+ 8.594	9.694	0.388	−11.63	36	72
19	0725	+13.475	8.919	0.3563	−10.69	36	78
20	0750	+18.919	8.182	0.3272	− 9.82	36	85
21	0835	+28.653	6.712	0.2685	− 8.06	48	78
22	0850	+33.181	6.202	0.2485	− 7.45	48	83
23	0905	+38.458	5.702	0.2285	− 6.85	48	84
24	0940	+54.861	4.645	0.1863	− 5.58	48	112
25	0955	+64.141	4.291	0.1720	− 5.16	48	121
26	1005	+71.136	4.109	0.1643	− 4.93	48	127
27	1030	+90.76	3.903	0.1565	− 4.69	48	133

center-to-limb Doppler frequency as well as the Doppler offset of the particular feature we want to lie at the center of the final map, that is, at $\xi = \eta = 0$. In the particular map we are concerned with, this was chosen to be the subradar point. The computed complex correlation functions are stored on magnetic tape in order of increasing Doppler angle φ.

Part two of the program reads all the complex correlation functions into core memory of the computer. For each run the Doppler angle φ_m must be read in and stored (Table II). The program must also be given information about the extreme values of ξ and η and the steps by which ξ and η must be incremented. Both the integrations over Θ and over φ in Eq. (27) of QPR (1966:3) are made by a simple trapezoidal method. The resulting matrix of powers $P(\xi, \eta)$ is stored on magnetic tape. The final step in the procedure is to correct for the antenna beam weighting and to produce a contour map by means of a standard contour program due to Stan Zisk of M.I.T. Other display methods have been attempted, notably an intensity-modulated CRT display, but so far without success. The resulting depolarized map of the moon is derived from the December data shown in Fig. 4.

D. Discussion

In order to identify some of the features in the map, the selenographic coordinate system was superimposed on the rectangular ξ, η grid system by making use of the transformation formula

$$\xi = \cos\delta \sin\lambda \cos\lambda_o - \cos\delta \cos\lambda \sin\lambda_o$$

$$\eta = \sin\delta \cos\delta_o - \cos\delta \cos\lambda \sin\delta_o \cos\lambda_o - \cos\delta \sin\lambda \sin\lambda_o \sin\delta_o \qquad (16)$$

where δ is the selenographic latitude and λ the selenographic longitude. The coordinates $(\delta_o \lambda_o)$ are those of the subradar point (assumed to remain fixed at $\delta_o = 5.3°S$ and $\lambda_o = 4.8°W$ throughout the run discussed here).

The most striking feature on the map, not unexpectedly, is the crater Tycho at (43°S, 11°W). In depolarized radiation this area appears significantly brighter than the subradar point. Even with this coarse resolution, the peak of the reflection at the crater Tycho is ten times higher than what it is in the regions of Mare Imbrium. Another striking feature is the aysmmetry in the contours near the subradar point. They appear to be displaced toward south-southeast. A glance at an optical picture of the moon shows that the area to the south of Sinus Medii appears more mountainous than that to the north. The crater Copernicus (10°N, 20°W) is quite definitely associated with a bulge in the contours and similarly, but less clearly so, the craters Theophilus (12°S, 27°E) and Aristarchus (24°N, 48°W).

It is also obvious that some of the marial regions appear quite dark, notably Serenitatis, Tranquilitatis, Imbrium and Procellarum. It is also interesting to note some peculiarities in the map. High reflectivity appears to be associated with Sinus Iridium or possibly with the Jura Mountains immediately to the north of it. The reflectivity in the southern hemisphere is higher than in the northern hemisphere. Furthermore, in the southern hemisphere reflectivity is higher in the western part than in the eastern part. The depolarized reflectivity from the areas to the southwest of Mare Humorum are anomalously bright, although there are no spectacular craters in this region. It should be observed that some of the contours extend beyond

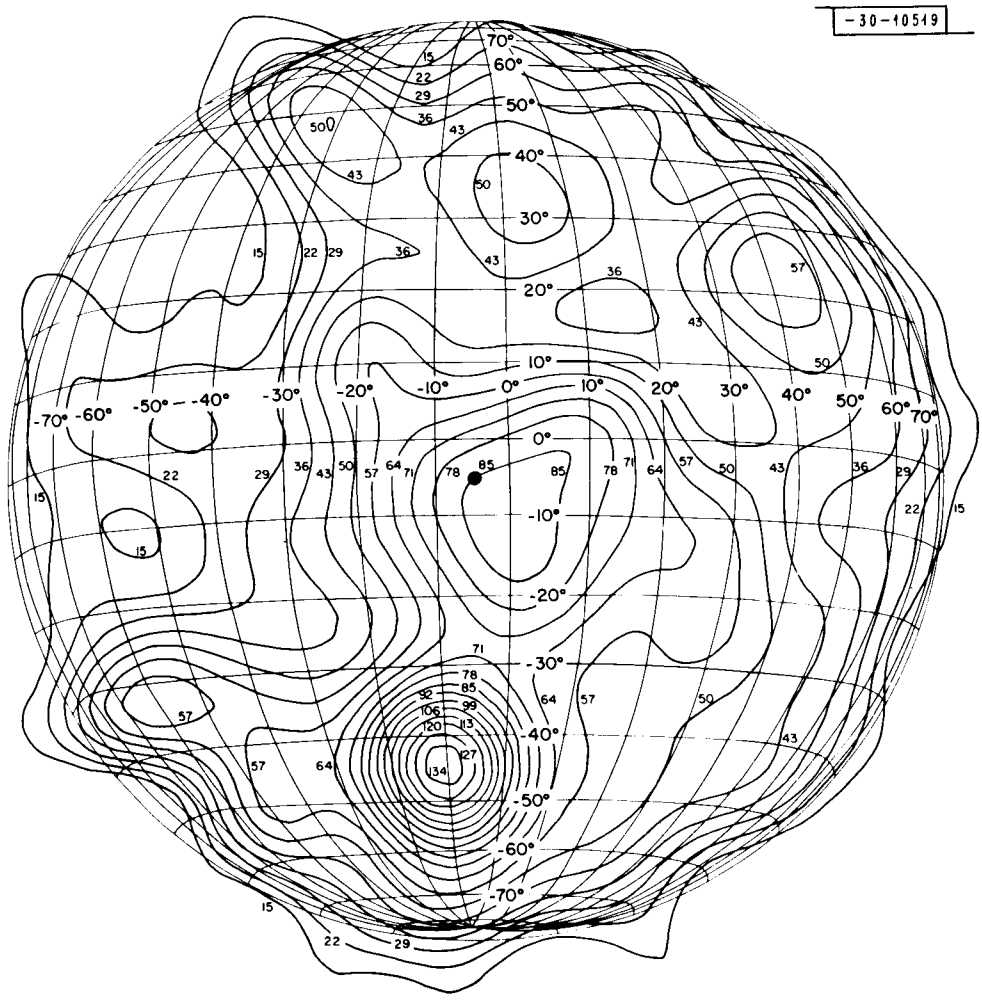

Fig. 4. Contour map of lunar reflectivity, depolarized circular component, 23-cm wavelength. Contours labeled in relative power.

the edge of the moon. This is primarily caused by the finite width of the equivalent polar diagram synthesized in the data processing.

On the whole we might conclude that there is good correlation between high depolarized reflectivity and bright mountainous regions, and between low reflectivity and dark marial regions. It is obviously desirable to increase the resolution in the map. The only reason this has not been done is that it would take excessive computer time. There are many ways of increasing the speed of the computations by including algorithms such as that due to Cooley and Tukey (1965) which would speed up the Fourier analysis of the data or by using a correlation and filtering unit to compute the complex autocorrelation function directly from the incoming data. This latter method would permit us to by-pass part one of the mapping program described above.

In its present form, the coherent mapping program can be used for detailed polarization studies of the moon to compare the depolarizing ability of maria, mountainous regions and other large scale features. In order to obtain satisfactory resolution near the edge of the moon, the coherent mapping technique can be applied range ring by range ring for both received polarizations. The depolarizing ability of different types of lunar material could then be studied by comparing the reflectivity of the polarized and the depolarized components along each range ring. These observations form part of a proposed extension to the Lunar Surface Studies contract between NASA and M.I.T. Lincoln Laboratory.

II. HIGH-RESOLUTION 3.8-CM REFLECTIVITY MAPPING

In mid-December 1966, the electronics necessary to pulse the new high-power Varian 949 klystron transmitting tubes had been completed and 3.8-cm radar mapping observations of the moon could be resumed. The use of the new transmitter at Haystack permitted substantially higher power (more than 200 kw), greater reliability and easier compatibility with other experiments. Along with this improvement, a computer program was written which permitted using the on-site CDC-3300 to take the data in a far more versatile format than previously. Continuous control of a local oscillator by the U-490 computer also removed the necessity of using a linear approximation to the Doppler shift, and permitted runs of long duration without frequency tracking error.

Measurements have been made on 21 and 22 December 1966 and on 24 and 31 January 1967. At the end of the current reporting period more than one-third of the equatorial region lying between ±16° latitude had been observed, including all Apollo landing sites except numbers 7, 9 and 10. According to the present schedule, more than three-quarters will have been completed by the end of February. As discussed in the original proposal, the resolution will vary from about 5 km in the central area of the lunar disk to about 2 km at high longitudes (or latitudes). An example from the central region surrounding the crater Copernicus is given in Fig. 5, where the grid spacing shown is one selenographic degree or approximately 30 km. Here the resolution is limited by the delay-Doppler mapping geometry to about 5 km. An example which lies farther from the center (Tycho) is shown in Fig. 6, where the grid spacing is in units of 1 percent of the lunar radius, or 17.4 km. The projection used in Fig. 6 corresponds closely to the aspect presented to an earth-based optical telescope, and may be compared with the accompanying optical photograph. In both Figs. 5 and 6, the differentiation in radar reflectivity appears to be controlled almost exclusively by local inclinations in the surface.

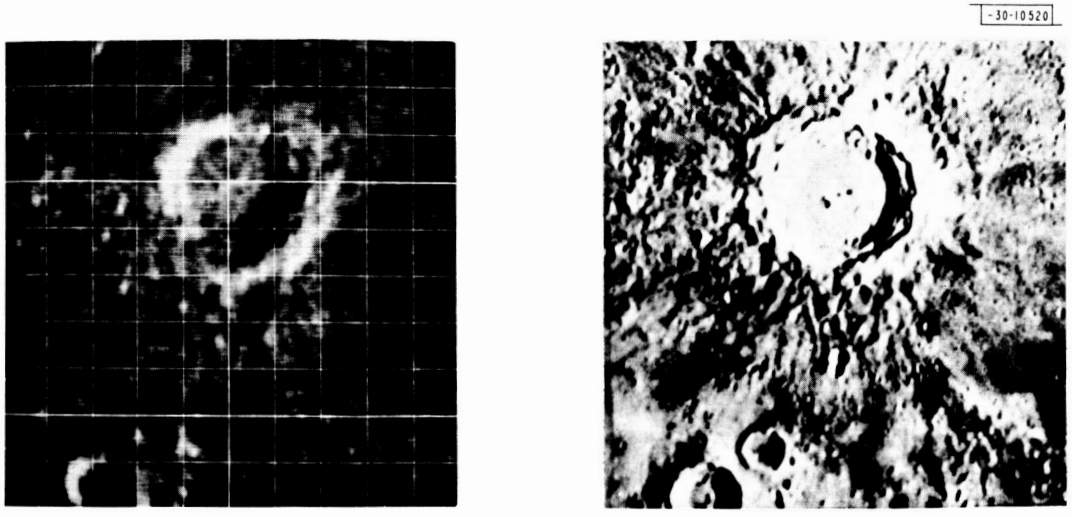

(a) (b)

Fig. 5. (a) 3.8-cm radar map of region surrounding lunar crater Copernicus. Map is nominally centered at 8°N, 20°W and the grid lines are at 1° intervals (30 km). Slight systematic bias in positions of all features may be noted which is connected with inaccuracies in current knowledge of lunar orbit and, perhaps, topography. (b) Optical photograph of same region (Rectified Lunar Atlas, University of Arizona Press, 1963).

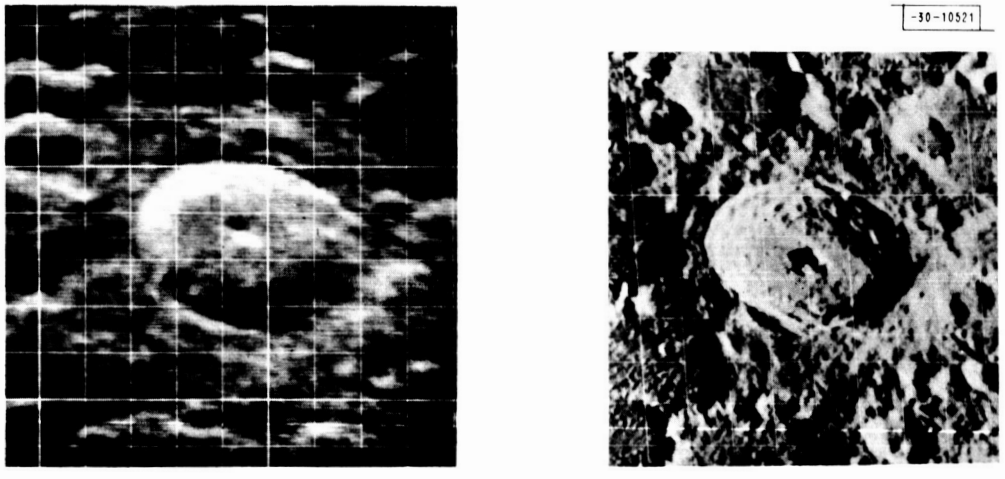

(a) (b)

Fig. 6. (a) High-resolution 3.8-cm radar map of lunar crater Tycho, direction cosine projection. Grid lines are spaced approximately 17 km. (b) Optical photograph of same region (Orthographic Atlas of Moon, University of Arizona Press, 1960).

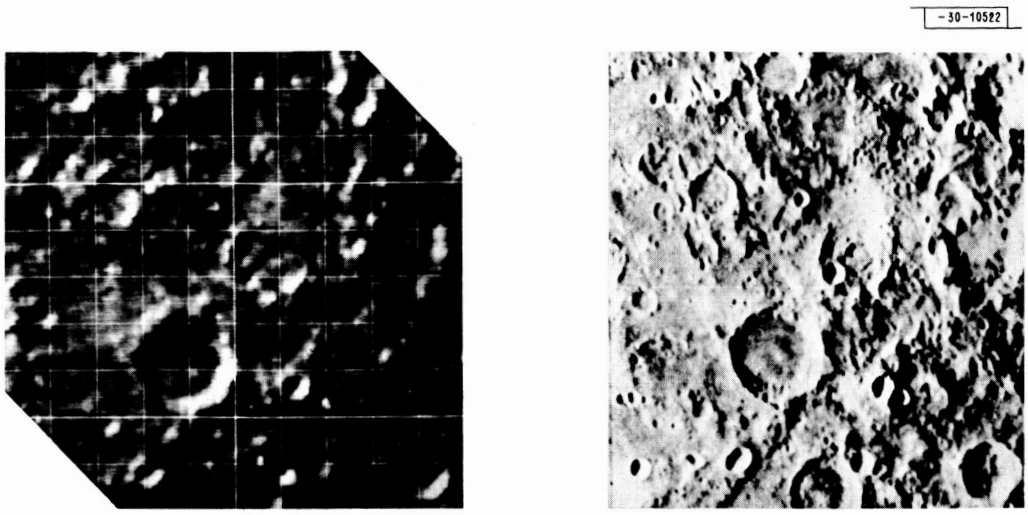

Fig. 7. (a) Preliminary 3.8-cm radar map centered at selenographic coordinates 12°S, 15°E, with grid spacing of 1° (30km). Large crater is Abulfeda. (b) Optical photograph of same region (Rectified Lunar Atlas, University of Arizona Press, 1963).

Figures 7 and 8 show in preliminary form portions of the lunar surface centered at selenographic 12°S, 15°E, and 4°S, 35°E, respectively. Here the resolution is about 3 km. Quite prominently visible left of center and near the top of Fig. 8 is an extended area in which the reflectivity is substantially higher than the average, although the local inclination, at least on a gross scale (as given by contours on Lunar Aeronautical Chart No. 79), is not particularly inclined to the local horizontal. A similarly enhanced region may be found near 6°S, 36°E. Both areas also show up as visually brighter in the accompanying photograph. On the other hand, a marial region located in the upper left corner of Fig. 8 displays a reflectivity, both visually and to the 3.8-cm radar, which is significantly below the average. It seems likely that the chief factor responsible for the variations in these latter cases is local roughness of the surface at the scale of 3.8 cm. Apollo site 2, which is located near the top of Fig. 8, appears unremarkable.

III. PROGRESS IN 8-MM RADAR SYSTEM

Shortly after the last quarterly report, the 8-mm radar detected echoes from the moon. This was done with a (nominally) 10-W klystron; the actual peak power radiated from the antenna feed line was 7 W. The pulse length was 2.4 seconds, and the receiver single-sideband noise figure was 13.6 dB. The signal was barely detectable on a single-pulse basis, as was to be expected on the basis of experience with a similar radar in 1963 (Lynn, et al., 1964).

A. Transmitter

After the moon had been detected, proving the radar's functioning as a system, there was a concentrated effort to increase the signal-to-noise ratio by increasing the power of the transmitter. Thus far, this effort has not been fully successful. The 10-W transmitter klystron

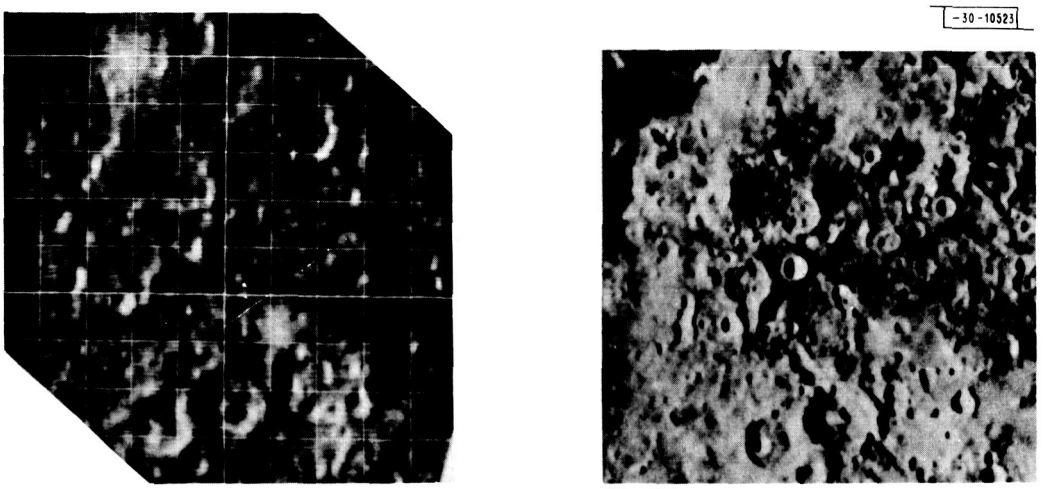

Fig. 8. (a) Preliminary 3.8-cm radar map centered at 4°S, 35°E with grid spacing of 1° (30 km). (b) Optical photograph of the same region (Rectified Lunar Atlas, University of Arizona Press, 1963).

has been replaced by one rated at 50 W, but difficulties have arisen in phase-locking this higher-power oscillator klystron to a crystal oscillator, in order to keep the signal within the 170-Hz bandwidth of the receiver. Two approaches are in progress: (1) to adapt the phase-lock system that succeeded with the 10-W tube; (2) to implement a new locking system that seems inherently better.

Phase locking control involves modulating the klystron beam voltage. Changing to the 50-W tube has demanded some redesign of the modulator to increase its dynamic range. After this revision, it became possible to phase-lock the 50-W tube for minutes at a time when it was connected to a dummy load. Shortly after the transmitter was connected to the antenna, failure of a piece of flexible waveguide produced violent standing waves in the RF system. Since then, for reasons not as yet understood, phase locking has become so difficult as to prevent operation of the radar. Concentrated effort is being centered on this problem.

With the phase-lock system now in use, any change in the transmitter tube, its operating point or its load demands a change in the crystal of the reference oscillator. Since the reference frequency must meet a tolerance of less than one part in ten thousand, changing crystals usually implies delay for procurement of a crystal, followed by further delay for stabilization of the oscillator after the crystal is in hand. Moreover, the phase reference in the present system does not have a satisfactorily pure spectrum; some of the transmitted power is wasted because it is not confined to a bandwidth as narrow as that of the receiver. This deficiency arises in part from noise in the output of the crystal oscillator, and in part from noise generated in the multiplier that converts from the oscillator frequency, about 11 MHz, to the transmitted frequency, about 35 GHz.

Improvements in the art since this radar was built now make possible a better phase reference. One can start with a highly stable fixed oscillator at 5 MHz, designed for low noise and containing in its output network a very sharply tuned filter to reduce the noise even further. The

multiplication from 5 MHz to about 35 GHz can be effected by multipliers less noisy than those now in use. Then a frequency synthesizer and single-sideband converter can, with little loss in purity of spectrum, translate this reference signal to the exact frequency at which the klystron is to be stabilized. Conceptually, the result is a phase reference that is far more rapidly adjustable and far cleaner in spectrum than the one now in use.

The critical items for implementing this scheme, the oscillator and the multiplier, have been procured (for driving the kilowatt transmitter that was planned at the outset of this program). A converter has been purchased, and a breadboard test of the concept is under way. The new scheme should provide an increase in effective transmitted power and also shorten the time required for adjustment of the transmitter. The only foreseen complication arises because, in order to employ a multiplier and a synthesizer that are actually available, it is necessary to do the frequency conversion at X-band, and then use a frequency tripler. The output of the X-band single-sideband converter has proved too weak to drive the tripler; it will therefore be used as reference for phase-locking an X-band klystron, which will in turn drive the tripler. For this purpose, a "lock box" usable at X-band has been obtained.

The problem of the 50-W transmitter is of importance now because the 1000-W transmitter that will supplant it is behind schedule, primarily due to administrative delays in procuring the 1000-W tube. Once approved, the development of the kilowatt tube progressed well, and was completed in the time span provided by the contract. The new tube is a six-cavity 35-GHz amplifier klystron, made by Varian Associates. It provides a gain of 53 dB and has run satisfactorily at a CW output of 1400 W at the plant. A transmitter which will contain this tube is under construction.

As soon as the 50-W transmitter can be phase-locked, observations of the moon will be resumed.

B. Other Developments

Except for its RF section, the receiver for dual polarization has been completed. Each channel has programmed compensation for Doppler shift and has, just before the output, a five-toothed comb filter. Each tooth of the filter has a 3-dB bandwidth of 170 Hz, and the teeth are centered at intervals of 100 Hz. The RF head for dual polarization has been constructed, an RF test bench for 35 GHz has been developed and testing of the waveguide components has begun.

Apart, perhaps, from the kilowatt klystron, the most critical components for improving the transmitter are the frequency multipliers. One of these will drive the klystron, at an input of 10 to 20 mW, and the other will provide local-oscillator power to the receiver mixers. To get 35 GHz from the excellent 5-MHz stable quartz oscillators that are commercially available, one must multiply the frequency by 7000, thereby incurring, in an ideal multiplier, a degradation of 77 dB in the signal-to-frequency modulating-noise ratio in the neighborhood of the desired frequency. To get the frequency increase entirely by a multiplier therefore demands that the multiplier be nearly ideal, because it is hard to get a 5-MHz source that has a signal-to-noise ratio appreciably better than 100 dB. Nevertheless, the conceptual and operating simplicity of direct multiplication from 5 MHz (as opposed, for instance, to multiplying by a smaller factor the output of a higher-frequency oscillator phase-locked to a 5-MHz reference) was so attractive that this method was selected a year ago to provide the transmitter and local-oscillator frequencies

for the kilowatt radar. Development and manufacture of the multiplier chains was undertaken by the Buffalo plant of Sylvania Electronic Products, Inc. Initial testing of these recently delivered all-solid-state devices shows that this crucial aspect of the RF development has been gratifyingly successful.

ACKNOWLEDGMENTS

The work of most of the technical personnel of Group 31, Surveillance Techniques, which operates the facilities of the Field Station, in preparing and conducting the work reported to date is gratefully acknowledged, as is the work of members of Group 46, Microwave Components, in cooperating with Dr. McCue on the 8.6-mm radar.

The use of the facilities of the Lincoln Laboratory Millstone-Haystack complex, provided by the U.S. Air Force, is also gratefully acknowledged.

REFERENCES

Bracewell, R.W., "Radio Astronomy Techniques," in Handbuch der Physik, Vol.LIV (Springer-Verlag, Berlin, 1962), pp 42-129.

Carpenter, R.L., "Study of Venus by CW Radar," Astron. J. 69, 2-11 (1964).

Cooley, J.W. and J.W. Tukey, "An Algorithm for the Machine Calculation of Complex Fourier Series," Math. Comput. 19, 90, 297-301 (April 1965).

Evans, J.V., R.P. Ingalls, L.P. Rainville and R.R. Silva, "Radar Observations of Venus at 3.8 cm Wavelength," Astron. J. 71, 902-915 (1966).

Hagfors, T., "A Study of the Depolarization of Lunar Radar Echoes," accepted for publication in Radio Science for May 1967.

Lynn, V.L., M.D. Sohigian and E.A. Crocker, "Radar Observations of the Moon at a Wavelength of 8.6 Millimeters," J. Geophys. Research 69, 781-783 (1964).